A EUROPEAN JOURNAL

CHEMPHYSCHEM

OF CHEMICAL PHYSICS AND PHYSICAL CHEMISTRY

Accepted Article

Title: Improving gas separation properties of PVAc-zeolite 4A mixed-matrix membranes through nano-sizing and silanation of the zeolite

Authors: Nazila Esmaeili, Sue Boyd, Chris L. Brown, Evan MacA Gray, and Colin J Webb

To be cited as: *ChemPhysChem* 10.1002/cphc.201900423

Link to VoR: http://dx.doi.org/10.1002/cphc.201900423

A Journal of ChemPubSoc Europe

WILEY-VCH www.chemphyschem.org

10.1002/cphc.201900423

Improving gas separation properties of PVAc-zeolite 4A mixed-matrix membranes through nano-sizing and silanation of the zeolite.

N. Esmaeili,[a] S. Boyd,[b] C. L. Brown,[b] E.MacA. Gray,[a] C.J. Webb*[a]

[a] Queensland Micro- and Nanotechnology Centre, Griffith University, Nathan 4111, Australia
[b] Environmental Futures Research Institute, Griffith University, Nathan 4111, Australia

Abstract: Mixed-matrix membranes containing synthesised nano-sized zeolite 4A and PVAc were fabricated to investigate the effect of zeolite loading on membrane morphology, polymer-filler interaction, thermal stability and gas separation properties. SEM studies revealed that, although the membranes with 40 wt% nano-sized zeolite particles were distributed uniformly through the polymer matrix without voids, the membranes with 15 wt% zeolite loading showed agglomeration. Thermal stability improved by zeolite content increase, and with increasing amount of zeolite nanoparticles the permeability decreased and the selectivity increased. The effect of silanation on dispersion of 15 wt% zeolite 4A nanoparticles through PVAc was investigated by post-synthesis modification of the zeolite with 3-Aminopropyl(diethoxy)methylsilane. Modification of the nanoparticles improved their dispersion in PVAc, resulting in higher thermal stability than the corresponding unmodified zeolite membrane. Modification also decreased the rigidity of the membranes. Partial pore blockage of the modified zeolite nanoparticles after silanation caused a further decrease in permeability, compared to the 15 wt% unmodified zeolite membrane.

[a] Ms N Esmaeili, Prof. E MacA Gray, Dr C J Webb*
Queensland Micro- and Nanotechnology Centre
Griffith University
Nathan 4111, Brisbane, Australia
*E-mail: j.webb@griffith.edu.au

[b] Dr S Boyd, Assoc Prof C L Brown
Environmental Futures Research Institute, Griffith University, Nathan 4111, Australia
Griffith University
Nathan 4111, Brisbane, Australia

1. Introduction

Hydrogen offers potential as a non-polluting energy vector that can be used to smooth the intrinsically intermittent energy production from renewable energy sources, such as wind and photovoltaic (PV) solar [1]. In various hydrogen-related applications, including electrolysers, PEM fuel cells, extraction of hydrogen from syngas, and CO_2 reduction or conversion, it is necessary to actively separate or maintain the separation of hydrogen from other gases, such as oxygen, nitrogen and carbon dioxide [2]. Environmental considerations, and relatively low energy consumption and cost compared to more established gas separation methods such as absorption and cryogenic distillation, have made membranes attractive for various gas separation applications, and there exists a need for commercially-feasible, high-performance membranes [3]. The gas separation performance of membranes is evaluated by the permeability of the gas molecules and their selectivity. The empirical upper bound for polymer membrane separation of gases, defined by Robeson [4], has limited further development of these membranes, due to permselectivities below this trade-off curve. Inorganic membranes such as zeolites, ceramic and carbon membranes have high thermal and chemical stability and higher permselectivity (beyond the Robeson upper bound) relative to polymeric membranes [5]. However, high cost and mechanical brittleness have constrained the application of inorganic membranes for industrial gas separation [3b, 6]. Combining the polymer with inorganic material to fabricate a mixed-matrix membrane (MMM) was proposed to incorporate the advantages of both materials and avoid their disadvantages, in order to achieve higher selectivity, permeability, or both, in comparison to pure polymeric membranes [3a, 7].

Various porous and nonporous inorganic fillers such as zeolite molecular sieves [7f, 8], carbon nanotubes [7b, 9], metal organic frameworks (MOFs) [10], zeolitic imidazolate frameworks (ZIFs) [7g], graphene oxide [11], titanium dioxide [12] and silica [13] have been used in MMM fabrication. Rubbery polymers are more flexible than glassy polymers and have better interaction with the inorganic phase, resulting in a membrane without voids at the interface between the polymer and filler [3a]. However, they typically have a high permeability and low selectivity compared to glassy polymers [14]. On the other hand, glassy polymers, despite the advantage of higher permselectivity, are more rigid and have lower compatibility with the inorganic filler surface, causing void formation at the organic-inorganic interface, bypassing the gas molecules through the voids and decreasing the selectivity, especially for higher loadings of inorganic filler [3a, 15].

Zeolites are three-dimensional crystalline microporous aluminosilicates, consisting of oxygen-sharing TO_4 tetrahedra, where T is Si or Al [16]. The TO_4 tetrahedra facilitate a monodispersed pore-size distribution with higher mechanical stability than amorphous materials [16a]. Linde type A (LTA) zeolite is composed of sodalite cages linked by 4-membered rings. A central large cavity, super cage or α cage, is formed by connection of the sodalite cages. Six similar cavities with a 8-ring window and opening diameter of 4.2 Å (β cages) are connected to the α cage [17]. The Si/Al ratio of a synthetic LTA type zeolite is approximately one, however, this ratio is higher when organic structure-directing agents (SDA) are used in nano-sized zeolite synthesis [18]. The 4A zeolite has a nominal pore size of 3.8 Å, making it suitable for separation of small gas molecules [3a], because of its molecular-sieve property, which allows for accurate size and shape discrimination [3a, 7f, 15b, 19]. It is advantageous for hydrogen separation as the hydrogen molecule is smaller than those in carrier gases. However, low compatibility between the polymer and zeolite surface can cause void formation at the interface of the polymer and zeolite, allowing the gas to bypass the sieve material, thus limiting application to gas separation [3a, 20]. Poly(vinyl acetate) (PVAc) has a low glass transition temperature, T_g, (35-45 °C) and is a flexible, low cost polymer with a high affinity to alumina, making it suitable for use with aluminosilicate zeolites, such as zeolite 4A, forming void-free MMMs [6b, 15e]. The combination of PVAc with micron-sized zeolite has shown good adhesion, making it a potential polymer for MMM fabrication studies [6b, 20b, 21]. The reported results for CO_2-CH_4 separation has motivated the use of MMMs based on PVAc for gas separation [21a].

Nano-sized zeolite has attracted attention because of a higher external surface area compared to micron-sized zeolites. Smaller particles shorten the diffusion path length, resulting in lower mass transfer resistance and higher selectivity [17]. For commercial MMMs, application of a *nano*-sized inorganic filler instead of micron-sized is necessary, as the selective layer of the asymmetric hollow fibre membranes needs to be thin (*ca* 100 nm) for best permeation [15d, 22], necessitating a nano-sized zeolite.

However, there are very few applications of nano-sized zeolites in MMMs reported in the literature, because of void formation at the polymer-zeolite interface caused by particle agglomeration [22c, 23]. Nano-sized inorganic materials tend to agglomerate, due to the difference between the physical and chemical properties of the polymer and inorganic phase and the interaction between the inorganic filler particles [23d, 24], which may form voids at the interface between the two phases and affect the gas permselectivity [22c, 25]. Perez *et al.* [26] fabricated MMMs by incorporation of nano-sized MOF-5. The characterisation of the morphology of the fabricated membranes showed agglomeration of the inorganic filler. Nevertheless, they did not observe any defects, due to the strong contact/interaction between the Matrimid® polymer used and the surface of the MOF-5 nano crystals. Zarshenas *et al.* [8a] prepared MMMs using nano-sized zeolite NaX incorporated into a Pebax–1657 matrix. Their MMMs with a low loading of zeolite nanoparticles (2 wt%) showed good dispersion without agglomeration, but increasing the zeolite content to 4 wt% resulted in agglomeration and void formation. Gas permeation results for the MMMs with nano-sized zeolites showed enhancement compared to the MMMs with micron sized zeolite particles. Although the zeolite loading was less than 4 wt%, the gas permeability of their membranes increased compared to the pure polymer membranes, but there was no increase in selectivity.

Better interaction of the inorganic filler with the polymer and reduced interaction between filler particles may lead to improved materials for gas separation. Modification methods such as silanation, Grignard treatment, low molecular weight additives (LMWA), annealing and priming have been applied to improve the morphology [6b, 15b, 15e, 20b, 20c, 22c, 27]. Surface modification of the zeolite nanoparticles by silane coupling agents could feasibly decrease the nanoparticle interaction, agglomeration and the repulsive forces between the polymer and zeolite phases, and so improve the compatibility of the zeolite and polymer [3a, 15c, 19a,

[20c, 28]. The purpose of this work was to investigate the effect of using nano-sized zeolite 4A particles on the membrane morphology and the gas separation performance. Where agglomeration was found, the surface silanation of zeolite nanoparticles was also studied to investigate the effect of modification on particle dispersion through the PVAc matrix, agglomeration prevention and to evaluate any change in gas separation performance. To the authors' knowledge, nano-sized zeolite particles have not previously been used to fabricate a MMM with PVAc polymer. Previous work on silanation in the literature has been on adhesion improvement between glassy polymers and micron-sized filler to reduce void formation. The effect of silane on zeolite 4A nanoparticle dispersion in PVAc has not yet been considered.

2. Experimental

2.1 Materials

To synthesize the zeolite NaA nanoparticles, colloidal silica (Sigma-Aldrich, Ludox@ TM-50, 50 wt% suspension in water), aluminium isopropoxide (Sigma-Aldrich, ≥98%), sodium hydroxide (NaOH) (Sigma-Aldrich, ≥98%) and tetramethylammonium hydroxide solution (TMAOH) (Sigma-Aldrich, 25 wt% in H_2O) were used. 3-Aminopropyl(diethoxy)methylsilane (APDEMS) (Sigma-Aldrich, 97%) and anhydrous toluene (Sigma-Aldrich, 99.8%) were employed for the surface silane modification of the nano-sized zeolite NaA. Poly(vinyl acetate) (PVAc) beads, (Sigma-Aldrich, average MW of 100000 and density of 1.18 g/ml at 25 °C) and anhydrous dichloromethane (DCM) (Sigma-Aldrich, ≥98%, containing 40-150 ppm amylene as a stabilizer, with bp= 39.8-40 °C and ρ=1.325 g/ml at 25 °C) were used for membrane fabrication. Anhydrous isopropanol and ethanol were used to wash the modified zeolite nanoparticles.

2.2 Nano-sized zeolite particle synthesis and modification

Zeolite 4A nanoparticles were synthesized by molar composition $1Al_2O_3{:}6SiO_2{:}0.16Na_2O{:}7.27(TMA)_2O{:}350H_2O$, as used by Jafari *et al.* [29]. After dissolving sodium hydroxide in deionized water (0.162 mol NaOH/L), TMAOH was added to the solution while stirring. Aluminium isopropoxide and colloidal silica were added to each half of the solution to prepare the aluminate and silicate solutions. When the solutions became clear, the silicate solution was gradually stirred into the aluminate solution. Aging took place at ambient temperature for 4 days while stirring, followed by crystallisation at 80 °C for 24 h. The synthesized zeolite 4A nanoparticles were collected by repeated cycles of centrifugation (10000 rpm) dispersion-ultrasonication until the pH was below 9. Finally, the nanoparticles were dried at 80 °C for 24 h, followed by calcination at 550 °C for 6 h in air to remove the TMAOH.

For silanation of the zeolite nanoparticles, 1 g of dried zeolite powder was dispersed into 100 ml toluene by ultrasonication, and stirred for 2 h. APDEMS (21 ml) was added to the zeolite solution while stirring under N_2 at 40 °C for 24 h. To remove the unreacted silane, the solution was centrifuged and washed with isopropanol and ethanol 3 times. Finally, the modified nanoparticles were dried at 80 °C overnight, followed by further drying under vacuum at 110 °C for 24 h.

2.3 Membrane fabrication

The solution casting method [21b] was used to prepare MMMs with varied amounts of unmodified zeolite 4A nanoparticles, 15 wt%, 30 wt% and 40 wt%, and 15 wt% of modified zeolite 4A nanoparticles ($W_{4A}/(W_{4A}+W_{PVAc})$). The polymer-zeolite solutions with 12–15 wt% total solid material ($W_{total\ solid}/(W_{total\ solid}+W_{DCM})$) were prepared for membrane preparation. This solid content in solvent was found to be optimal, as lower concentrations led to sedimentation of the filler particles, and higher concentrations did not disperse the particles properly. The zeolite nanoparticles and PVAc were vacuum dried for 24 h at 520 °C and 100 °C, respectively. The weighed zeolite nanoparticles were dispersed in DCM, alternating vigorous stirring with ultrasonication at least four times, for 1 h each time. Separately, PVAc was dissolved in DCM to make the polymer solution. Immediately after the final ultrasonication, about 20 wt% of the PVAc solution was added to the zeolite solution while mixing vigorously to prime (stabilize) the zeolite nanoparticles solution dispersion overnight. The remainder of the PVAc solution was added to the zeolite solution and stirred for 2 h. Then the solution was mixed on a roller at 60 rpm for 3–4 days for homogenisation before degassing under vacuum and casting on a Teflon plate. Finally, the solution was cast with a casting knife with a 100–200 µm gap. The film was covered with a pin-holed aluminium foil and dried naturally for two days under DCM-saturated atmosphere at ambient temperature to decrease the solvent evaporation rate, before transferring to a vacuum oven for further drying for one day at ambient temperature to remove any residual solvent. After that, the film was annealed at a temperature above the glass transition temperature (T_g) of the PVAc to maintain the flexibility of the polymer and decrease the stress at the interface of the polymer and zeolite. The temperature was varied based on the zeolite content: 50 °C for 15 wt%, 65 °C for 30 wt% and 80 °C for 40 wt%. This was chosen because the stress at the interface of the polymer and zeolite increases with increased amount of zeolite. Higher temperatures help to alleviate the effect of the higher loading of the inorganic filler on the stress accumulation during membrane drying and provide more mobility to the polymer in order to have better access to any inaccessible regions between the zeolite and remove defects at the polymer-zeolite interface [15e, 30]. Finally, the film was cooled slowly to room temperature under vacuum. As a reference, a pure PVAc membrane was prepared with the same method without the zeolite dispersion.

3. Characterisation

3.1 Nano-sized zeolite characterisation

The purity and crystallinity of the synthesised zeolite nanoparticles were determined by X-ray diffraction (XRD) using a GBC MMA X-ray diffractometer ($Co_{K\alpha}$ λ=1.78897 Å, 28.5 kV, 35 mA). Scans were taken over a 2θ range of 5–50° in

continuous scanning mode with a step size of 0.02° and a scan speed of 0.2 s per step. To analyse the structure of the unmodified and modified zeolite 4A nanoparticles, Fourier Transform Infrared spectroscopy (FTIR) scans were taken with a Perkin Elmer Spectrum FT-IR Spectrometer, from 400-4000 cm^{-1} with a resolution of 4 cm^{-1}. The particle size and morphology of the particles were evaluated by Scanning Electron Microscopy (SEM) (JSM-7100F). The microscope included an X-ray detector for energy-dispersive X-ray spectroscopy (EDS) elemental analysis. Thermogravimetric analysis (TGA) was performed using a NETZSCH STA 449 F3 thermal analyser under nitrogen, with temperatures ranging from 25-800 °C at a heating rate of 10 °C/min, to evaluate the degree of silanation. Solid state ^{29}Si (59.9 MHz) and ^{13}C (75 MHz) Cross Polarisation Magic-Angle Spinning (CPMAS) and ^{29}Si Bloch Decay Magic-Angle Spinning (BDMAS) nuclear magnetic resonance (NMR) experiments were carried out to investigate the modified and unmodified zeolite nanoparticles. The Brunauer-Emmett-Teller (BET) surface area was obtained using a Micromeritics TriStar II 3020.

3.2 Membrane characterisation

The structure of each membrane was evaluated by Fourier Transform Infrared spectroscopy (FTIR) using a Perkin Elmer Spectrum in the range 400-4000 cm^{-1} with a resolution of 4 cm^{-1}. The surface and cross-section morphology of the membranes were characterised by SEM with a JEOL JSM-7100F. The membranes were fractured by immersing in liquid nitrogen and coated with gold, before performing the cross-sectional measurements. Thermal stabilities of the membranes were investigated by thermogravimetric analysis (TGA) (NETZSCH STA 449 F3). The membranes were heated under nitrogen to 800 °C at a heating rate of 10 °C/min. The same instrument was used to perform Differential Scanning Calorimetry (DSC) under nitrogen from 25 to 100 °C (10 °C/min) to investigate the rigidity of the membranes. The thickness of the membranes was measured with a digital micrometer to a resolution of 1 µm. The measured thickness for each membrane was the average of at least 10 different locations through the membrane surface.

3.3 Pure gas permeation measurement

Gas permeation measurements were made using the constant-volume-variable-pressure method [7e] with a purpose-built membrane cell. The permeability is determined from equation (1) [11], by measuring the steady state increase in the permeate pressure with time (*dp/dt*):

$$P = \frac{VlV_m}{ART(p_f - p_p)}\frac{dp}{dt}\times 10^{10} \quad (1)$$

where the permeability, *P*, is in Barrer, (1 Barrer=10^{-10} cm^3_{STP} cm/cm^2 *s cmHg*), *V* is the volume of the permeate side (cm^3), *l (cm)*, the membrane thickness, V_m, the molar volume *(cm^3/mol)*, *A (cm^2)*, the membrane surface area, *T (K)*, the temperature, p_f, and p_p the feed and permeate pressures *(bar)*, respectively, and R *(6236.56 cm^3cmHg/mol K)*, the universal gas constant.

The ideal selectivity for gas pairs A and B is determined by the following equation [9]:

$$\alpha_{AB} = \frac{P_A}{P_B} \quad (2)$$

where, P_A and P_B are the permeabilities of gases *A* and *B* respectively.

The schematic of the stainless steel membrane cell is shown in Figure 1. Two O-rings with appropriate chemical and thermal resistance were used, one to seal the cell from the outside environment and the other to seal the membrane between the feed side and the permeate side. To mechanically support the membrane, a porous sintered stainless steel 316L plate (1 µm average pore size, 54% porosity and 1 mm thickness) (Tridelta Siperm GmbH, Germany) was used. The membrane was protected with standard filter paper (pore size of 11 µm) between the sintered metal plate and the membrane. A flat stainless steel ring (1 mm thickness) was used to clamp the membrane directly onto the permeate side. A schematic of the full gas permeation apparatus is shown in Figure 2. The permeation cell was immersed in water in a refrigerated/heating circulator (Julaba, FP45-HE), both to accurately control the temperature and to allow the measurements to be done at different temperatures.

After loading a membrane and connecting the membrane cell back into the permeation apparatus, both permeate and feed sides were evacuated for at least 24 h before the permeation measurements. He, H_2, N_2 and CO_2 were used sequentially during the pure gas permeation measurements. A GE Druck UNIK 5000 pressure transducer with accuracy 0.04% of full range was used to record the permeate side pressure. The effect of temperature on permeability was investigated by measuring the permeability at 30 °C, 40 °C and 50 °C, with a differential pressure of 0.75 bar. Reproducibility was checked by performing the permeation experiments at least twice for each membrane.

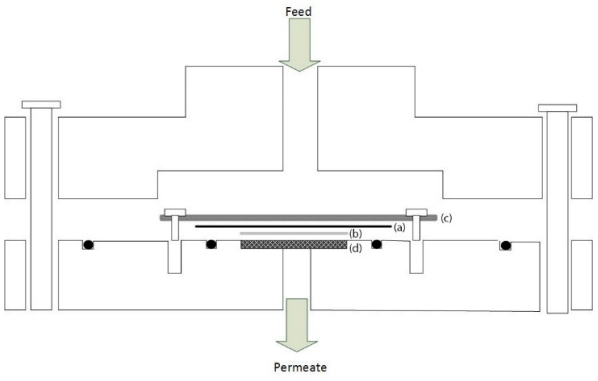

Figure 1. Schematic of membrane cell cross-section: (a) membrane, (b) filter paper, (c) stainless steel ring (membrane holder), (d) sintered metal plate

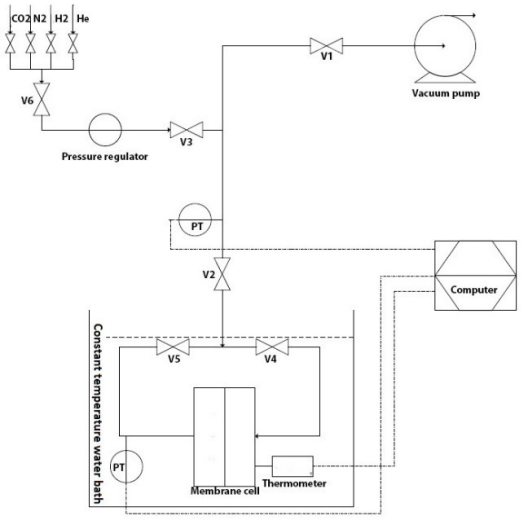

Figure 2. Schematic of the pure gas permeation apparatus

4. Results and discussion

4.1 Zeolite 4A nanoparticles

Figure 3a shows an XRD pattern of the as-synthesised zeolite nanoparticles. Peak fitting using HighScore Plus software provides a good match with pure zeolite LTA, from the peak positions. Peak intensities varied, most likely due to preferred orientation.

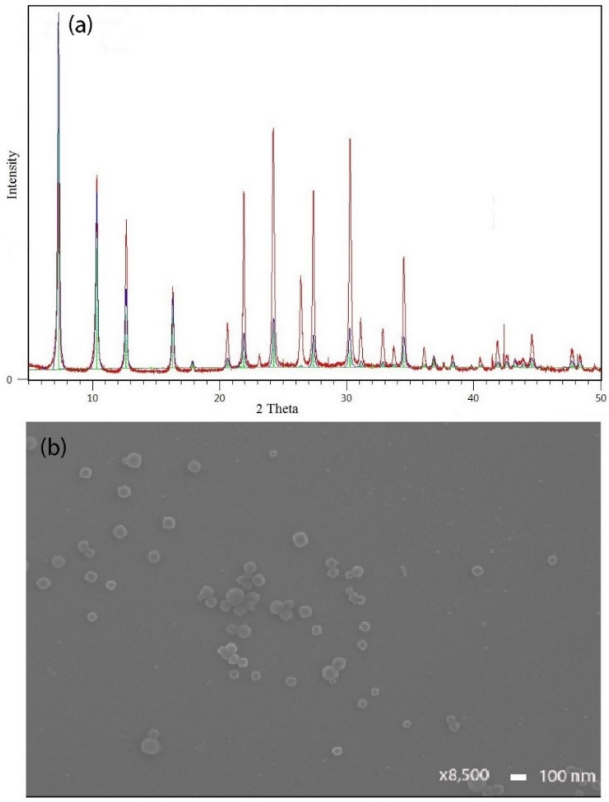

Figure 3. (a) XRD patterns and (b) SEM image of the nano-sized zeolite 4A

From the SEM image of the zeolite nanoparticles (Figure 3b), the average particle size was observed to be ~100 nm, with a particle size distribution of 50–120 nm. The elemental analysis of the synthesised zeolite 4A nanoparticles is shown in Table 1. The Si/Al ratio (1.44) is consistent with the literature [31].

Table 1. EDS elemental analysis of the synthesised zeolite 4A nanoparticles

Element	Atomic Concentration [%]	Mass Concentration [%]
Oxygen	62.71	50.36
Sodium	8.9	10.27
Aluminium	11.94	16.17
Silicon	16.45	23.2
Total	100	100

4.2 Zeolite 4A nanoparticle modification

Solid state NMR was used to characterise the materials in terms of their functional groups. ^{29}Si (59.9 MHz) and ^{13}C (75 MHz) CPMAS

spectra were obtained for both modified and unmodified zeolite 4A nanoparticles to evaluate the presence of APDEMS in the modified zeolite 4A nanoparticles. CPMAS is a line narrowing technique that utilises ^{1}H-X cross polarisation for the signal enhancement of the less sensitive X resonances. Resonant intensities are inherently biased in a CPMAS experiment; the resonances of nuclei that are (a) close in space to ^{1}H nuclei and (b) in relatively immobile molecular environments will be significantly enhanced relative to nuclei in more isolated and/or more mobile environments. ^{29}Si BDMAS experiments were also conducted on the samples. BDMAS also uses MAS line narrowing, but these experiments were simple one pulse experiments. Cross polarisation was not used for signal enhancement, so the resulting Bloch decays do not exhibit CP intensity bias. The intensities of resonances observed in ^{29}Si BDMAS experiments reflect the relative concentrations of all ^{29}Si environments present in the bulk of the zeolite.

Alkyl resonances in the ^{13}C CPMAS spectrum of the zeolite may appear due to either a residue of TMAOH from the synthesis of the zeolite, or from the silanation with APDEMS. The ^{13}C CPMAS spectrum of the modified zeolite (M1-M4) in Figure 4 showed that APDEMS derived material was present in the modified zeolite. These alkyl resonances were not present in the spectra of the unmodified zeolite nanoparticles, demonstrating TMAOH was removed completely by calcination. From ^{29}Si BDMAS of the unmodified and modified zeolite 4A in Figure 5, it can be seen that the majority of ^{29}Si nuclei resided in similar chemical environments in both unmodified and modified zeolites. However, by narrowing the line in ^{29}Si CPMAS, a broad resonance, δ ~(–15) - (–25) ppm (the peak shown as T1 in Figure 5), appeared in the modified zeolite 4A nanoparticles spectra which was not present in the unmodified zeolite spectra (Figure 5). This suggests that some of the alkyl material was located within immobilised D type functionality, such as [–O-Si(R)$_2$-O-silicate] functionality, demonstrating zeolite modification.

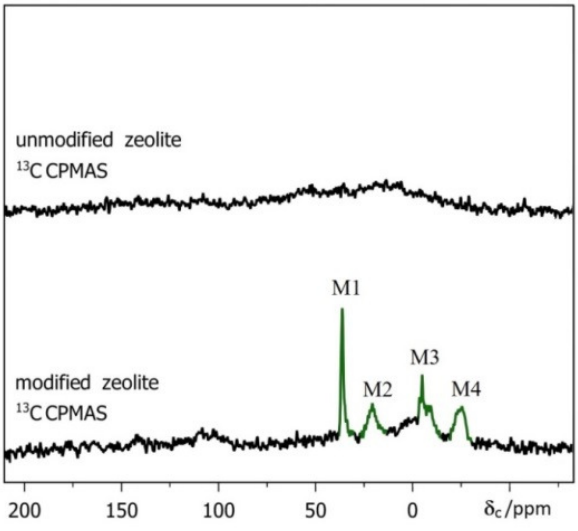

Figure 4. 13C CPMAS spectra of the modified and unmodified zeolite 4A nanoparticles

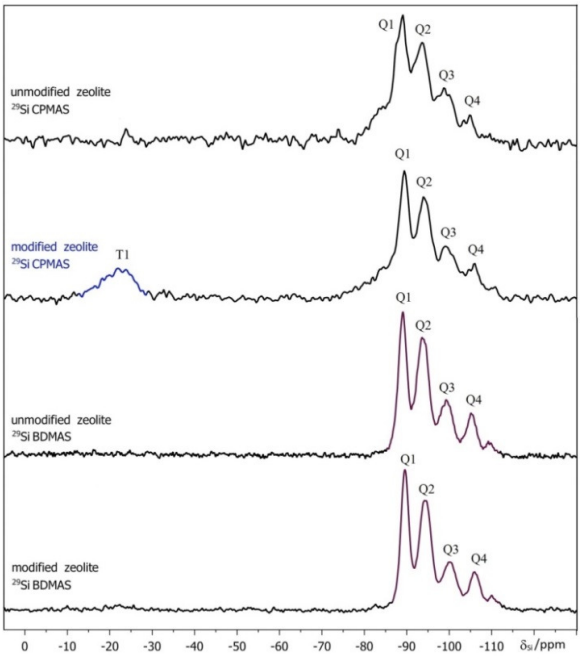

Figure 5. ^{29}Si CPMAS and ^{29}Si BDMAS spectra of the modified and unmodified zeolite 4A nanoparticles

Figure 6 shows TGA curves of the modified and unmodified zeolite 4A nanoparticles, performed to estimate the content of functional groups attached to the surface of the material after modification. The weight loss below 300 ℃ in both the modified and unmodified zeolites corresponds to water and solvent adsorbed inside the pores [32]. Increasing the temperature over 400 ℃ revealed an additional step in the decomposition of the modified zeolite, compared to the TGA curve for the unmodified zeolite, resulting in about 1 % weight loss, which could be attributed to the decomposition of the silane, which is consistent with the literature [27a, 32b, 33].

FTIR spectroscopy in the mid-infrared region was performed to investigate the molecular interaction and structural changes of the zeolite phase after silanation. In Figure 7, plot (a), which shows the FTIR spectrum of the unmodified zeolite 4A, the absorption bands at 468 cm^{-1}, 556 cm^{-1}, 674 cm^{-1}, 992 cm^{-1} and 3389 cm^{-1} are attributed to the characteristic bands of zeolite 4A, in good agreement with the literature [16b, 18a, 34]. The bands at 471 cm^{-1}, 674 cm^{-1} and 992 cm^{-1} correspond to bending, symmetric stretching and asymmetric stretching vibrations of the internal tetrahedral (T–O bond in TO_4, where T is Si or Al), respectively. The band at 3383 cm^{-1} indicates the inner hydroxyl group stretching vibrations [16b, 18a, 34]. The band at 555 cm^{-1} corresponds to the vibrations of D4R, the main secondary building unit in LTA-type zeolite [35]. Figure 7, plot (b), shows a FTIR spectrum of the modified zeolite 4A nanoparticles, which has additional peaks at 1251 cm^{-1}, 1385 cm^{-1} and 2982 cm^{-1}, compared to the unmodified zeolite 4A, as have been previously observed with silanation of micron sized zeolites [27a, 33, 36]. There are also shifts in wavenumber and changes in intensity and width of the peaks, in comparison to the spectra of unmodified zeolite 4A. The peak at 2982 cm^{-1} is assigned to the aliphatic C–H (CH_2, CH_3) stretching vibrations, and the peak at 1251 cm^{-1}

and 1385 cm^{-1} correspond to the Si–CH_2 and Si–CH_3 stretching vibrations, respectively [20a, 36b]. These bands suggest good adherence of silane to zeolite surface [36a]. There are several overlapping bands such as the N–H bending and stretching vibrations. The N–H stretching vibration of the primary amine in silane is located in the wavenumber range 3300-3500 cm^{-1}, which overlaps with the O–H stretching vibrations of hydroxyl groups in zeolite, resulting in a weakened spectra and a shift from 3389 cm^{-1} to 3379 cm^{-1}, suggesting the presence of silane [27a]. The peak at 1643 cm^{-1} in the FTIR spectra of the modified zeolite nanoparticles is broader with lower intensity than the peak at 1641 cm^{-1} in FTIR spectra of the unmodified zeolite nanoparticles, which suggests the presence of N–H bending vibrations of the silane group (ranging 1590-1620 cm^{-1}) overlapped with the band in the zeolite structure [27a]. The asymmetric stretching vibration of the internal tetrahedral bond in zeolite 4A underwent a significant change in band intensity, width and a peak shift after modification. The peak is narrower than that of the unmodified zeolite and shifted from 992 cm^{-1} to 978 cm^{-1}. In addition, other peaks showed a slight shift to lower wavenumbers after modification. These changes suggest a strong interaction between APDEMS and zeolite 4A nanoparticles without significant change to the zeolite structure. The BET surface area of the zeolite nanoparticles decreased from 628 m^2/g to 491 m^2/g with silanation, which could be due to the pore blockage by silane, as silane is mobile and has access to the zeolite pores during the modification [37].

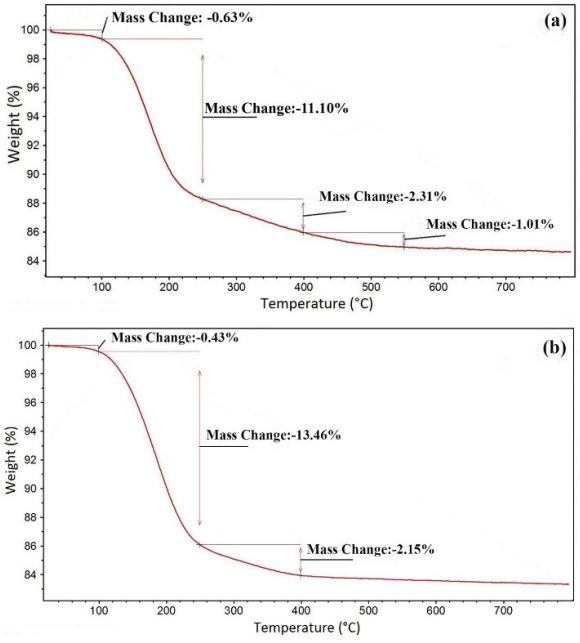

Figure 6. TGA curves of the (a) modified and (b) unmodified zeolite 4A nanoparticles

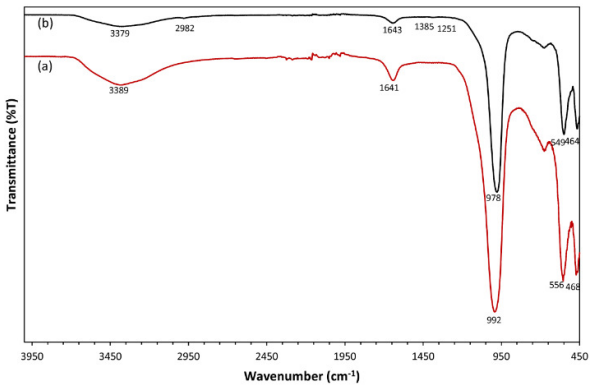

Figure 7. FTIR spectra of (a) unmodified zeolite 4A and (b) modified zeolite 4A nanoparticles

4.3 Membrane characterisation

4.3.1 MMMs comprising unmodified zeolite 4A nanoparticles

4.3.1.1 FTIR analysis

To investigate the molecular interaction and the changes in the structure of the membrane due to the addition of the inorganic fillers, FTIR spectra of the pure PVAc membrane and MMMs with various percentages of zeolite nanoparticles were performed. Figure 8(b) shows FTIR spectra of the fabricated membranes. From the spectrum of the pure PVAc membrane, strong peaks at 1728 cm^{-1} and 1224 cm^{-1} correspond to the acetate carbonyl (C=O) and C–O stretching vibrations [38], and the bending vibrations of the C=O are seen at 633 cm^{-1} and 660 cm^{-1}. The asymmetric deformation vibrations of the CH_3 and CH_2 groups are found at 1370 cm^{-1} and 1430 cm^{-1}. The bands at about 2970 cm^{-1}, 2850 cm^{-1}, 2923 cm^{-1} and 2721 cm^{-1} are assigned to the asymmetric and symmetric stretching vibrations of C–H in CH_3 and CH_2 groups, respectively [39]. When the zeolite nanoparticles were added to the PVAc, matrix, the characteristic bands of zeolite 4A appeared. For MMMs incorporating 15 wt% zeolite nanoparticles, the peaks are at 467 cm^{-1}, 556 cm^{-1}, 668 cm^{-1} and the broadened peak at 3455 cm^{-1}. In addition, there is a change in intensity and width of the bands compared to the spectra of PVAc membrane, especially between 850 cm^{-1} and 1200 cm^{-1}, the asymmetric band which characterises the stretching vibrations of TO_4 in the zeolite structure. By increasing the zeolite 4A content to 40 wt%, the bands related to the zeolite 4A intensified, while the vibrations of acetate group of PVAc weakened. In addition, the band at 1018 cm^{-1} shifted significantly to lower frequency close to the band of TO_4 in zeolite 4A, creating a broad peak at 994 cm^{-1} suggesting that the acetate groups on PVAc have interacted strongly with the silanol groups of zeolite 4A [40].

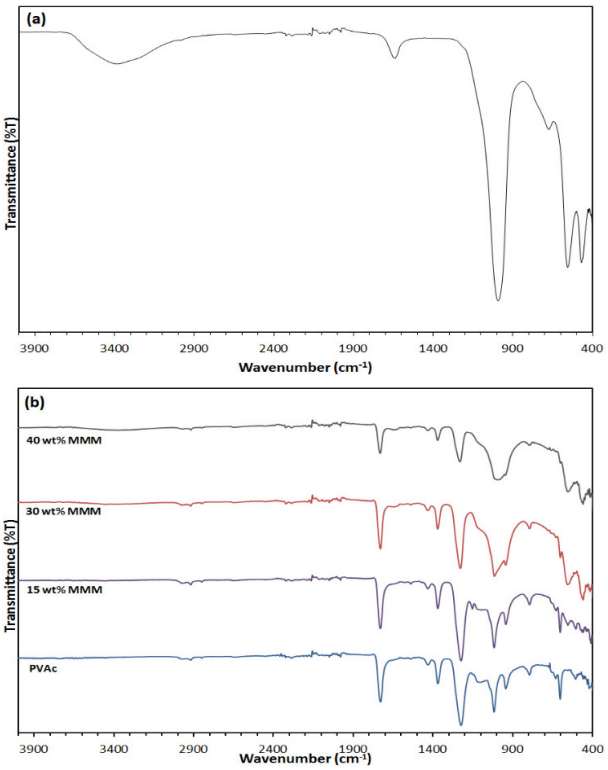

Figure 8. FTIR spectra of (a) zeolite 4A nanoparticles (b) pure PVAc membrane and MMMs containing zeolite nano-sized zeolite 4A

4.3.1.2 Thermogravimetric Analysis (TGA) and Differential Scanning Calorimetry (DSC)

TGA was performed to investigate the thermal stability of the fabricated membranes and the effect of zeolite nanoparticles on the thermal stability. From the results shown in Figure 9, three decomposition steps were seen in all membranes. A small amount of weight loss at temperatures below 250 °C is attributed to the loss of adsorbed water from the membranes. This may be due to adsorption of moisture from the air during sample preparation for the TGA experiment. Other researchers have also reported similar weight loss at low temperatures [41]. This weight-loss is higher for larger amounts of the hydrophilic zeolite 4A nanoparticles in the membrane matrix and points to water adsorbed by the zeolite. The next two weight-loss events are ascribed to decomposition of the PVAc. During the degradation process of PVAc, a series of complex free radical reactions including the rearrangements and scissions of the polymer chain may occur [41a]. The side chain groups may be eliminated at the first stage of the polymer degradation (excluding any water loss). Polyalchene structures, which are produced as a result of the reaction in the first polymer degradation step, decompose during the second degradation step [41a, 42]. In addition, a residue with conjugated double bonds may be formed during the de-acetylating process [41a, 43]. This residue is pyrolysed weakly at the last weight-loss stage [41a]. From the TGA results, the prepared pure PVAc membrane started to decompose at about 283 °C and continued with the majority of weight loss (70 %) occurring by 385 °C. Acetic acid is eliminated from the PVAc side groups at this stage [41a]. About 25 % of the polymer backbone degraded at temperatures between 385–520 °C. These results are consistent with the literature [6b, 41a, 44]. In the MMMs, as the amount of zeolite nanoparticles increased, the onset temperature of the polymer decomposition increased slightly from 292 °C for 15–wt% zeolite to 309 °C for 40–wt% zeolite. This increase in the degradation onset temperature with increasing zeolite content shows an enhanced thermal stability, which may be attributed to restriction of the polymer motion because of the interaction between the polymer and zeolite, as well as a greater amount of energy needed for polymer chain movement and segmentation [27a, 41c]. This suggests a favourable interaction between the PVAc and zeolite 4A nanoparticles.

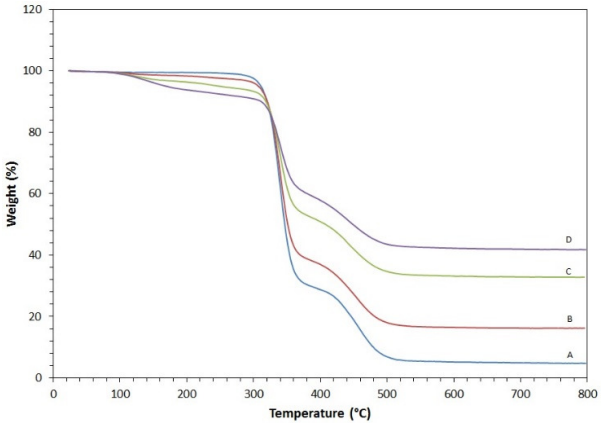

Figure 9. TGA of (A) PVAc, (B) 15 wt% 4A MMM, (C) 30 wt% 4A MMM, (D) 40 wt% 4A MMMs

The glass transition temperature, T_g, is a qualitative estimation of the polymer chain flexibility, and can be used to investigate the interaction between the polymer and inorganic filler and the polymer chain rigidity at the interface of the zeolite and polymer for different zeolite loadings [3a, 45]. As Figure 10 shows, all the mixed-matrix membranes had a single T_g, indicating an effective interaction between the zeolite nanoparticles and PVAc on a molecular level, for all zeolite loading levels. In addition, a decrease in the polymer chain mobility near the zeolite-polymer interface and rigidification of the polymer chains because of the generated shrinkage stresses during solvent removal is confirmed by an increase in T_g with the addition of the inorganic filler to the polymer matrix [15d, 20b, 45-46]. During membrane preparation, as the solvent is removed in the film formation, shrinkage stresses at the zeolite-polymer interface are created, which cause the polymer chains to lose their mobility [47]. With the addition of zeolite nanoparticles to the PVAc matrix, T_g of the membrane increased about 5 °C and 6 °C for membranes containing 15 wt% and 30 wt% zeolite nanoparticles, respectively, compared to the pure PVAc membrane. The membrane with 40 wt% zeolite loading had almost the same T_g with the membrane containing 30 wt% zeolite nanoparticles, in accordance with the literature. Previous reports indicated that beyond a certain amount of zeolite, further increase in the zeolite content did not affect T_g [48]. It was suggested that only a certain amount of zeolite may act as a chain rigidification agent, because of the heterogeneous nature of the MMM morphology [48]. In addition, the increased annealing temperature with increasing zeolite nanoparticle content applied in this work may have reduced both the stresses at the zeolite-polymer interface and rigidification.

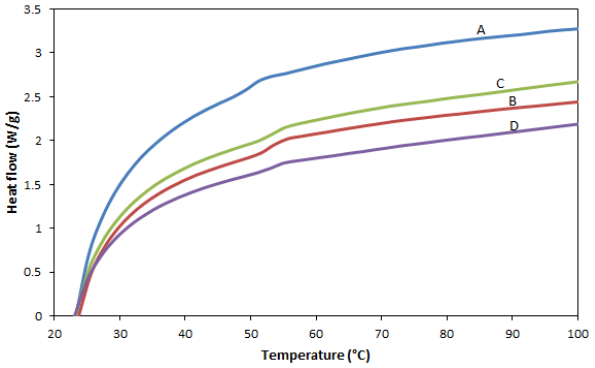

Figure 10. DSC curves (A) PVAc, (B) 15 wt% 4A MMM, (C) 30 wt% 4A MMM, (D) 40 wt% 4A MMMs

4.3.1.3 Scanning electron microscopy (SEM)

The cross-sectional SEM images of the pure PVAc membrane and MMMs with various zeolite nanoparticle loading are shown in Figure 11. Incorporation of 15–wt% nano-sized zeolite 4A into the PVAc matrix, formed island-like structures, due to the tendency of nanoparticles to agglomerate. The size of the islands increased with zeolite loading making a connected structure with better distribution of the zeolite. However, there was no evidence of void or defect formation at the zeolite-PVAc interface of both the isolated nanoparticles and the continuous domains of nanoparticles. This morphology was also observed by Huang *et al.* [23b], where the MMMs formed island-like structures with the incorporation of nano-sized zeolite 4A into a polyether sulfone matrix. The authors suggested that the zeolite nanoparticles create a second continuous phase without any void or defect formation at the interface of the polymer and zeolite.

The structure of the filler, priming, and the annealing process are likely reasons for an absence of voids in the membrane. Priming the zeolite surface improves the interaction of the zeolite and polymer. Although the zeolite nanoparticles have a strong tendency to agglomerate, their semi-spherical structure helps the PVAc, which has a high affinity to alumina [15e], to infiltrate the spaces between the nanoparticles and thus cover and encapsulate the nanoparticles with a thin layer by interacting with the silanol groups of the zeolite 4A. In addition, annealing provides mobility to the polymer chain during the solvent removal, resulting in better access of the polymer to any inaccessible regions between the zeolite nanoparticles, and relaxing defects at the zeolite-polymer interface [15e]. Kim and Marand [49] reported the fabrication of MMMs with incorporation of MCM-48 into a polysulfone phase. The fabricated membranes showed the formation of domains due to agglomeration at 20 wt%. However, the isolated particles and continuous domain did not have any defects or voids, and were well coated with polymer. They reported that weakly acidic surface silanol groups covered the mesoporous MCM-48, which enhanced the interaction with the organic polymer. As a result, the permeability of the fabricated membrane increased, with a slightly decreased or constant selectivity.

As is shown in Figure 11(g,h), with increasing zeolite content to 40 wt%, the zeolite nanoparticles were more uniformly distributed through the PVAc compared to membranes with lower zeolite content, and the particles completely interacted with the PVAc without any agglomeration. Possible reasons for better distribution of the zeolite nanoparticles at higher loading could be the lower viscosity of the casting solution and a stronger interaction between nanoparticles at lower contents of zeolite, which have both been previously reported [15f, 40]. Clarizia *et al.* [15f] also observed lower homogeneity of the membranes and increased sedimentation at lower percentages of micron-sized zeolite particles in polydimethylsiloxane (PDMS) matrix compared to the membranes with higher zeolite loading. They attributed this to viscosity and density differences between the particles and polymer, and the interaction between the zeolite particles. Some fracture lines from freezing in liquid nitrogen, and cavities from the SEM beam, can also be observed in Figure 11. This has also been reported by other researchers [49-50].

SEM images of membrane surfaces are shown in Figure 12. The pure PVAc membrane had a smooth surface. Addition of the zeolite 4A nanoparticles increased the roughness of the fabricated membranes. The zeolite nanoparticles appeared to be distributed fairly uniformly through the membrane, although there were island-like structures, especially at lower zeolite loading. These results are consistent with the cross-sectional SEM measurements.

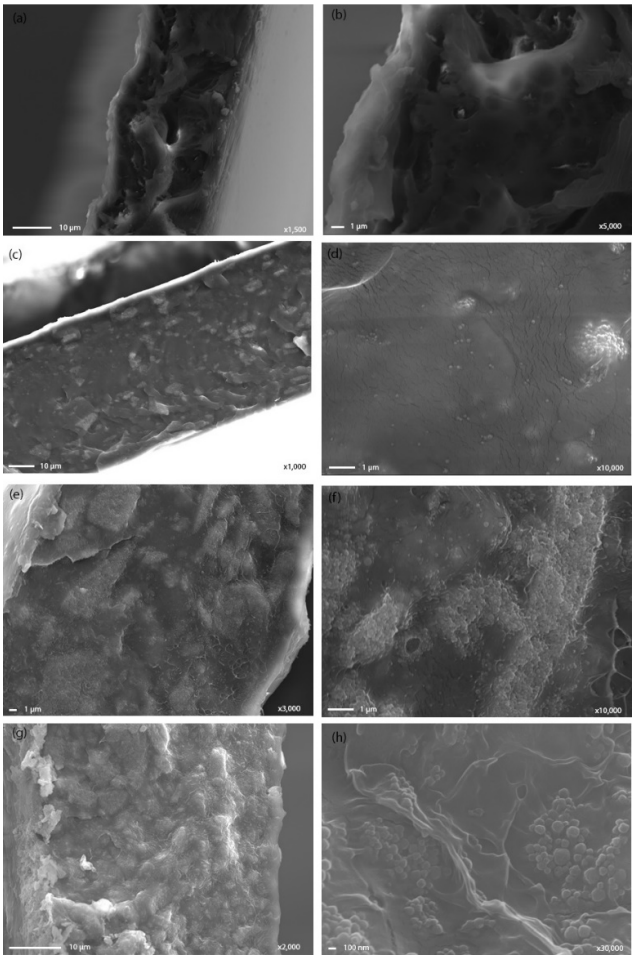

10.1002/cphc.201900423

Figure 11. The cross sectional SEM images of (a,b) the pure PVAc membrane, (c,d) 15 wt% 4A MMM, (e,f) 30 wt% 4A MMM, (g,h) 40 wt% 4A MMM

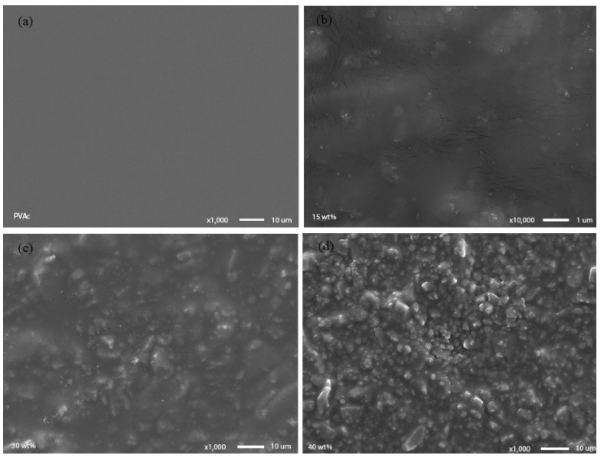

Figure 12. The surface images of the (a) pure PVAc membrane, (b) 15 wt% 4A MMM, (c) 30 wt% 4A MMM, (d) 40 wt% 4A MMM

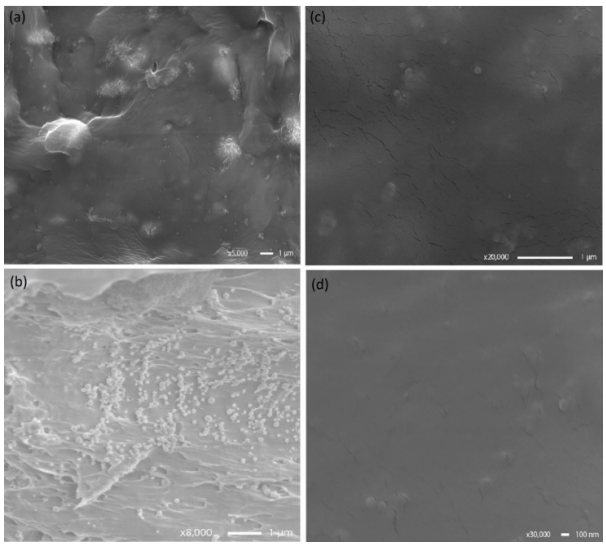

Figure 13. SEM images for 15 wt% unmodified zeolite 4A MMM cross-section (a) and surface (c), and 15 wt% modified zeolite 4A MMM cross-section (b), and surface (d).

4.3.2 MMM comprising 15 wt% modified zeolite 4A nanoparticles

The zeolite 4A nanoparticles were silanated to investigate the effect of surface modification on nanoparticle dispersion through the polymer matrix in MMM, as the fabricated MMM containing lower amount of unmodified zeolite nanoparticles (15 wt%) showed agglomeration. Figure 13 shows the SEM cross-sectional and surface images of the MMMs incorporating 15 wt% unmodified and modified zeolite 4A nanoparticles. It is evident from the SEM images of the membrane containing modified zeolite 4A nanoparticles in Figure 13b,d, that the silanated zeolite nanoparticles are dispersed uniformly through the membrane matrix with negligible agglomeration, showing that silanation of the zeolite 4A nanoparticles improved the morphology of the fabricated membrane.

TGA was performed to investigate the effect of zeolite silanation on thermal stability of the membrane (Figure 14). For the unmodified MMM, the onset temperature for polymer decomposition was ~292 ℃, compared to the modified zeolite MMM degradation temperature of about 302 ℃. This improvement in thermal stability may be explained by the strong interaction between PVAc and zeolite 4A, which restricts the PVAc movement. As a result, a higher energy is required for polymer chain segmentation and movement [27a, 41c]. This may be attributed to the interaction of the hydroxyl groups of zeolite surface with the silane groups of APDEMS and the interaction of the amine group of the APDEMS with PVAc [27a].

Figure 15 shows the DSC curve of the unmodified and modified MMMs, as well as the pure PVAc membrane. Similar to the unmodified MMMs, the modified MMM exhibited just one T_g, which is an indication of a good interaction between the zeolite 4A nanoparticles and polymer on the molecular level [6b]. The glass transition temperature of both MMMs with unmodified and modified zeolite 4A nanoparticles were higher than that of the pure PVAc membrane, suggesting a decrease in polymer chain mobility in the vicinity of the zeolite-polymer interface and rigidification of the polymer chains due to shrinkage stresses generated during solvent removal [15c, 20b, 45]. However, the T_g of the MMM comprising the silanated zeolite 4A nanoparticles was lower than that of the MMM with unmodified nanoparticles, showing that the modification of the zeolite particles could be effective in reducing the extent of the polymer-zeolite interface rigidification.

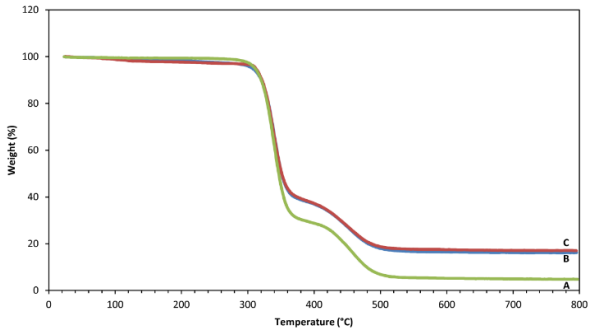

Figure 14. TGA of (A) pure PVAc membrane, (B) 15 wt% unmodified zeolite 4A MMM, (C) 15 wt% modified 4A MMM

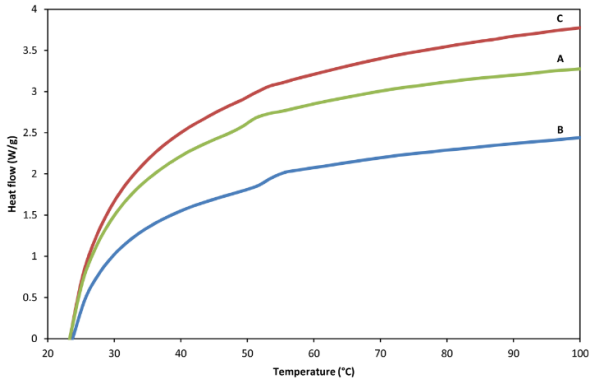

Figure 15. DSC curve of (A) pure PVAc membrane, (B) 15 wt% unmodified zeolite 4A MMM, (C) 15 wt% modified zeolite 4A MMM

4.4 Gas permeation experiments

Tables 2 and 3 show the pure gas permeability and gas pair selectivity of the fabricated membranes at different temperatures. The effect of zeolite loading on gas permeability and selectivity of membranes is shown in Figures 16 and 17. By addition of unmodified zeolite nanoparticles to the polymer matrix, the permeability of all gases decreased with a significant increase in selectivity, compared to the pure PVAc membrane. Increasing the amount of zeolite nanoparticles to 40 wt% resulted in the highest permeability reduction and selectivity enhancement. The decrease in permeability for N_2 and CO_2 were much higher (47.54% and 38.87% for MMM comprising 40 wt% zeolite nanoparticles) than He and H_2 permeability decrease percentage (23% and 17%), showing that the zeolite 4A nanoparticles were effective as a molecular sieve. Zeolite 4A nanoparticles with a pore size of ~3.8 Å separate gas molecules based on their size, shape or transition state selectivity [23b]. Moreover, the permeability results confirm the absence of voids within the membrane. According to the Maxwell model, the permeability in an ideal membrane without any defect, rigidification or pore blockage should increase slightly with a significant increase in selectivity relative to the slow gases. However, based on the nature of the polymer and the inorganic filler, and the polymer chain rigidification at the interface of the polymer and filler due to stresses during the membrane preparation, partial pore blockages or voids at the polymer-filler interface may cause the membranes to have a different gas permselectivity from that predicted by the Maxwell model. The modified Maxwell model [21b] was used to investigate the effects of various parameters on the gas permselectivity. The reduction in gas permeability was attributed to chain rigidification in the vicinity of the zeolite-polymer interface, and also to the partial pore blockage of the inorganic filler with polymer [21b]. As the membranes showed higher T_g compared to the pure PVAc membrane, the reduction in permeability could be attributed to the rigidification of the polymer chains at the vicinity of the zeolite nanoparticles [6b, 15e, 45]. However, partial pore blockages at low temperature could also explain the permeability reduction. J. Ahmad and M.-B. Hägg [6b, 30] used micron-sized zeolite 4A for fabrication of MMMs with a PVAc polymer. According to their results, the highest zeolite loading obtained without any defects was 25 wt%, with membranes with higher zeolite content having some voids. They attributed the void formation to the membrane preparation procedure. The nano-sized zeolites used in this work could increase the gas permselectivity of MMMs more than micron-sized zeolites, due to higher diffusivity in nano-sized particles. This could be explained by the difference in the Si/Al ratio of the nano and micron-sized zeolite 4A particles. By increasing the Si/Al ratio, the number of cations in the zeolite channels and cells is reduced. The cations have strong effect on the interaction and diffusion of gas molecules with the zeolites. Higher cation content results in stronger attractive forces between the zeolite surface and the gas molecule, which may make transport of the gas molecules through the zeolite channels difficult. On the other hand, lower cation content increases the gas molecule diffusion and permeability [23b, 51]. As nano-sized zeolite 4A particles have higher Si/Al ratio (Si/Al=1.44) compared to the micron-sized zeolite 4A particles (Si/Al=1), they could facilitate gas diffusion and permeation through the membrane.

Table 2. The gas permeability of membranes (in Barrer) with different zeolite nanoparticle content and modified zeolite nanoparticle at different temperatures and 0.75 bar pressure across the membrane.

Temperature	**30 ℃**				**40 ℃**				**50 ℃**			
Membrane	P_{He}	P_{H2}	P_{CO2}	P_{N2}	P_{He}	P_{H2}	P_{CO2}	P_{N2}	P_{He}	P_{H2}	P_{CO2}	P_{N2}
PVAc	9.13	5.84	1.24	0.061	13.41	9.27	2.56	0.132	18.48	13.84	4.86	0.327

15 wt% unmodified LTA-MMM	8.59	5.75	1.08	0.049	11.97	8.44	1.63	0.082	17.04	12.93	3.77	0.203
30 wt% unmodified LTA-MMM	7.81	5.3	0.87	0.038	11.08	7.86	1.49	0.073	15.76	11.09	3.14	0.163
40 wt% unmodified LTA-MMM	7.02	4.85	0.76	0.032	9.84	7.04	1.21	0.06	13.63	10.48	2.42	0.125
15 wt% modified LTA-MMM	8.15	5.55	0.907	0.0388	10.63	7.41	1.32	0.066	15.22	11.35	3.23	0.161

Table 3. The gas pair selectivities of the membranes with different zeolite nanoparticle content and modified zeolite nanoparticle at different temperatures and 0.75 bar pressure across the membrane.

	T **℃**	**Selectivities**				
Membrane		H_2/N_2	H_2/CO_2	CO_2/N_2	He/N_2	He/CO_2
PVAc	30	95.74	4.71	20.33	149.67	7.36
	40	70.23	3.62	19.39	101.59	5.24
	50	42.32	2.85	14.86	56.51	3.80
15 wt% unmodified LTA-MMM	30	117.35	5.32	22.04	175.31	7.95
	40	102.93	5.18	19.88	145.98	7.34
	50	63.69	3.43	18.57	83.94	4.52
30 wt% unmodified LTA-MMM	30	139.47	6.09	22.89	205.53	8.98
	40	107.67	5.27	20.41	151.78	7.44
	50	68.04	3.53	19.26	96.69	5.02
40 wt% unmodified LTA-MMM	30	151.56	6.38	23.75	219.37	9.24
	40	117.33	5.82	20.17	164	8.13
	50	83.84	4.33	19.36	109.04	5.63
15 wt% modified LTA-MMM	30	143.04	6.12	23.38	210.05	8.99
	40	112.21	5.61	20	161.01	8.05
	50	70.49	3.52	20.05	94.53	4.71

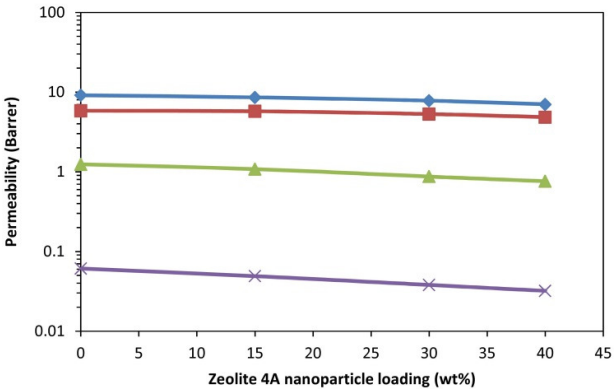

Figure 16. Zeolite loading effect on pure gas permeability. (♦) He, (■) H_2, (▲) CO_2, (×) N_2. (T=303.15 K, p=0.75 bar)

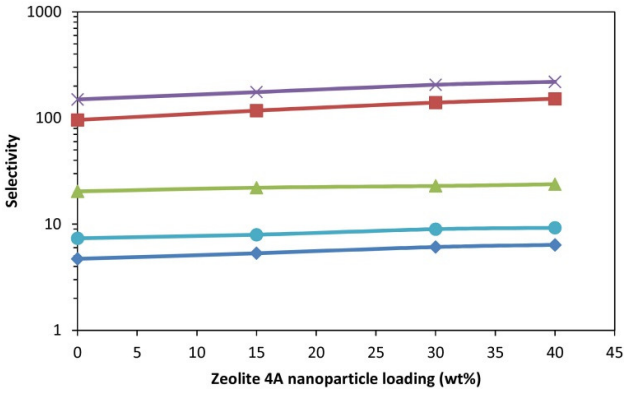

Figure 17. Zeolite loading effect on selectivity. (♦) H_2/CO_2, (■) H_2/N_2, (▲) CO_2/N_2, (×) He/N_2, (●) He/CO_2. (T=303.15 K, p=0.75 bar)

The effect of temperature on gas permselectivity of the MMM containing 40 wt% zeolite 4A nanoparticles is shown in Figure 18 and Figure 19. As can be seen, the permeability of all gases increased with increasing temperature, reaching 13.63 Barrer (He), 10.48 Barrer (H_2), 2.42 Barrer (CO_2) and 0.125 Barrer (N_2) at 50 ℃. However, all gas-pair selectivities decreased with increasing temperature, to 83.84 (H_2/N_2), 4.33 (H_2/CO_2), 19.36 (CO_2/N_2), 109.04 (He/N_2) and 5.63 (He/CO_2) at 50 ℃.

Temperature dependency of gas permeation through dense polymeric membranes can be described by an Arrhenius-type equation:

$$P = P_0 \exp(\frac{-E_p}{RT}) \quad (3)$$

while the diffusivity (D) and selectivity (S) are:

$$D = D_0 \exp(\frac{-E_d}{RT}) \quad (4)$$

$$S = S_0 \exp(\frac{-\Delta H_s}{RT}) \quad (5)$$

where E_p, E_d and ΔH_s are the permeation activation energy, the diffusion activation energy and the heat of sorption, respectively. Diffusivity increases with increasing temperature. Small non-reacting gases such as N_2, He and H_2 have a small positive value of adsorption heat, which means the solubility also increases slightly with temperature [6b]. For more condensable, i.e. non-ideal, gases such as CO_2, the heat of adsorption is negative, and their permeability is dependent on their diffusivity [6b, 52]. The activation energy could be used to investigate the effect of temperature on the degree of permeability increase for different gases and the change in selectivity. The activation energy is higher for gas molecules with larger kinetic diameter [6b, 53], such that N_2 has the highest activation energy and He has the smallest activation energy among the gases investigated in this work. From the Arrhenius-type equation, higher activation energy results in higher permeation change with temperature [15f]. As a result, larger gas molecules are more affected by temperature increase. As Figure 18 shows, N_2 had the highest permeability increase with temperature, which is consistent with the higher activation energy. This resulted in a reduction in selectivity of the other gases relative to N_2, as the rate of increase in permeability of other gases was lower than that of N_2. In addition, the slope of the H_2/CO_2 and He/CO_2 selectivity was increased from 40 ℃ to 50 ℃. This may be due to the state of PVAc at temperature below and above the T_g (~45 ℃). The gas permeability through PVAc membrane in the glassy state is affected more by the diffusion coefficient than the solubility, and as a result, gas molecules such as H_2 and He show higher permeability increase with temperature than CO_2 [6b]. In the rubbery state, the permeability is more greatly affected by the solubility coefficient than the diffusion coefficient, and the solubility of the more condensable gas CO_2 is higher [6b]. Therefore, by increasing the temperature to 50 ℃, CO_2 permeability increase rate is higher, resulting in lower selectivity.

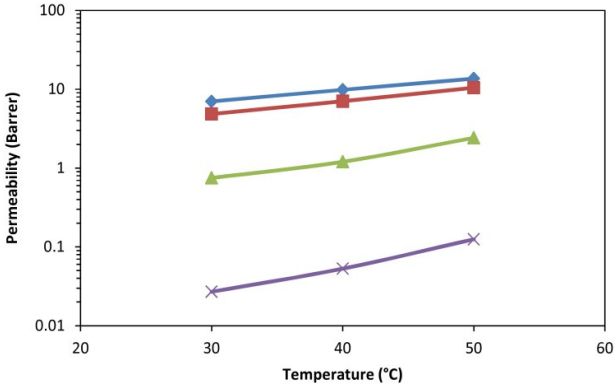

Figure 18. Effect of temperature on pure gas permeability of MMM containing 40 wt% zeolite 4A nanoparticles. (♦) He, (■) H_2, (▲) CO_2, (×) N_2

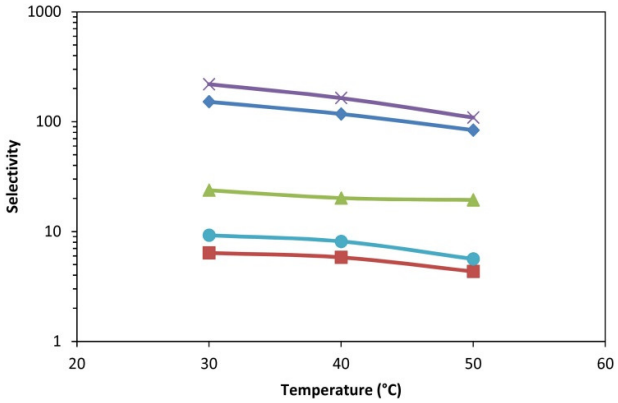

Figure 19. Effect of temperature on gas pair selectivity of MMM containing 40 wt% zeolite 4A nanoparticles. (♦) H_2/N_2, (■) H_2/CO_2, (▲) CO_2/N_2, (×) He/N_2, (●) He/CO_2

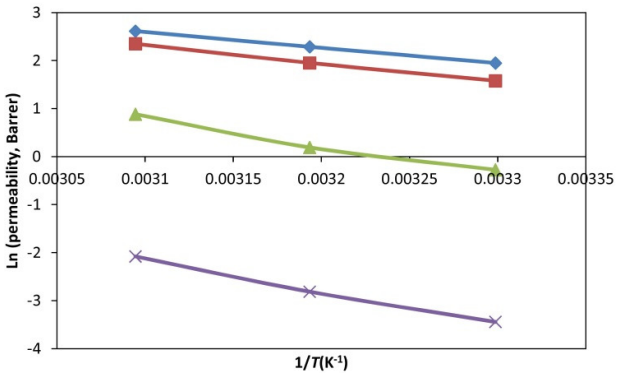

Figure 20. Arrhenius-type plot of the permeability of MMM containing 40 wt% zeolite 4A nanoparticles. (♦) He, (■) H_2, (▲) CO_2, (×) N_2

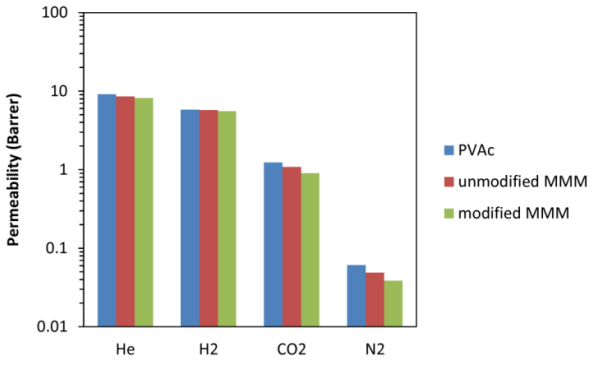

Figure 21. Pure gas permeabilities for pure PVAc membrane, 15 wt% unmodified zeolite 4A nano MMM and 15 wt% modified zeolite 4A nano MMM (*T*=303.15 K, *p*=0.75 bar)

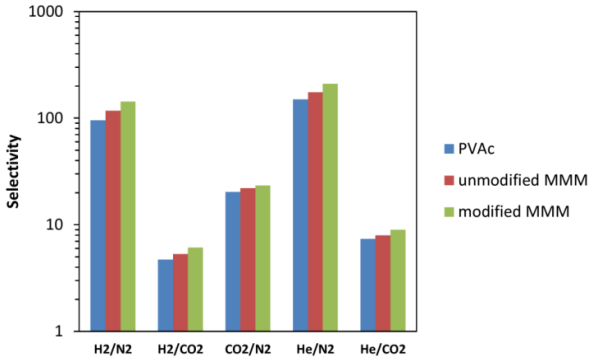

Figure 22. Gas pair selectivities for pure PVAc membrane, 15 wt% unmodified zeolite 4A nano MMM and 15 wt% modified zeolite 4A nano MMM (*T*=303.15 K, *p*=0.75 bar)

Figures 21 and 22 show the permeability of He, H_2, CO_2 and N_2 and gas pair selectivities, respectively, of pure PVAc membrane and MMMs containing 15 wt% unmodified and modified zeolite 4A nanoparticles at 30 °C and 0.75 bar. The permeability of all gases decreased and the selectivities increased, for both MMMs, compared to the pure PVAc membrane. MMM containing modified zeolite 4A nanoparticles showed lower permeabilities than MMM with unmodified zeolite 4A nanoparticles, due to the zeolite nanoparticle pore blockage by silane, which was further supported by a decrease in BET surface area of zeolite nanoparticles with modification. Reduction of the zeolite surface area due to pore blockage by silanation was reported previously [37].

The effect of temperature on the permeability and selectivity of MMMs containing unmodified and modified nano-sized zeolite 4A particles is shown in Figure 23 and Figure 24. By increasing the temperature, the permeability of all gases increased, with a decrease in gas pair selectivities, as shown in Tables 2 and 3.

From Table 2 and 3, comparing the gas permeation and selectivity of the MMMs containing 15 wt% modified zeolite nanoparticles and 40 wt% unmodified zeolite nanoparticles shows that the 15 wt% modified zeolite MMM had higher permeability with a slightly lower selectivities. Using lower nano-sized zeolite with the similar gas separation performance decreases the cost of synthesis. In addition, the membranes with lower content of zeolite nanoparticles are more flexible than those containing higher zeolite content.

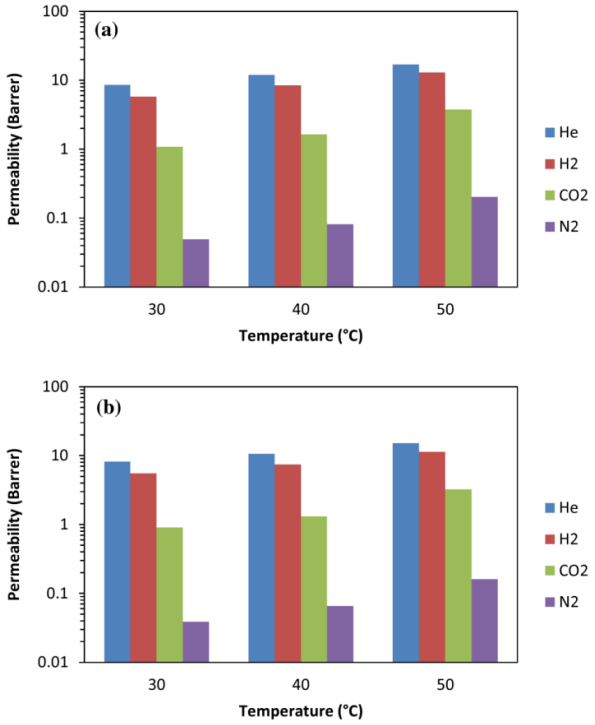

Figure 23. Effect of temperature on pure gas permeabilities of MMM containing 15 wt% (a) unmodified and (b) modified zeolite 4A nanoparticles

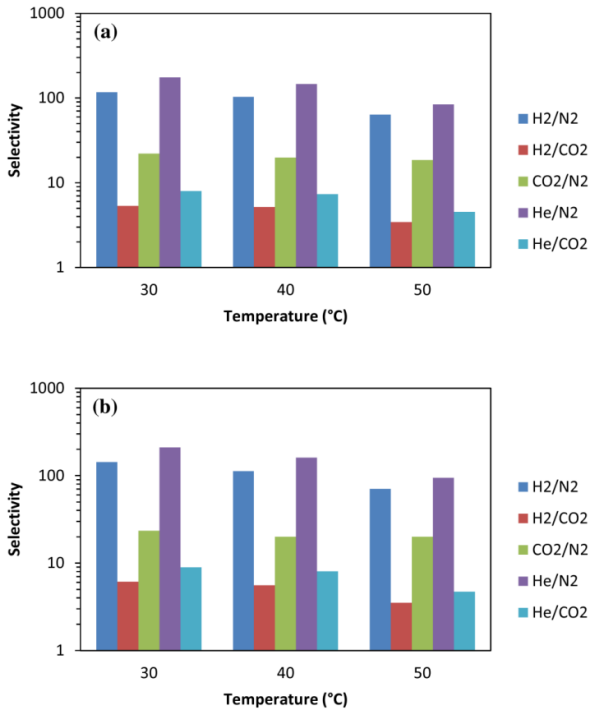

Figure 24. Effect of temperature on gas pair selectivity of MMM containing 15 wt% (a) unmodified and (b) modified zeolite 4A nanoparticles

Table 4 summarises the gas separation performance of MMMs with different polymers and zeolite nanoparticles from the literature. For comparison with this work, the gas separation performance of MMMs fabricated with *micron*-sized zeolite 4A and PVAc is shown. Except for CO_2, the permeability values in this work are slightly higher than those membranes fabricated using micron-sized zeolite 4A and PVAc, because of higher diffusivity of the nano-sized zeolite over micron-sized zeolite. However, the selectivities were slightly lower. The difference in CO_2 permeability was due to the feed operating pressure, which was higher in the literature. We performed the permeation experiments at 0.75 bar, in order to avoid the CO_2-plasticisation tendency of PVAc [21a]. Plasticisation at 8 bar is known to cause an increase in CO_2 permeability [6b, 30]. The experiments performed by Ahmad and Hägg [6b] showed an increase in CO_2 permeability from about 0.85 Barrer at 2 bar to 2.78 Barrer at 8 bar in the MMMs containing 15 wt% micro-sized zeolite 4A, an increase attributed to CO_2 plasticisation [6b]. Although the gas separation results in the literature vary due to different polymer types, zeolite type, zeolite loading and permeation operating conditions, our results show that PVAc MMMs containing nano-sized zeolite 4A particles could have potential in hydrogen and other gas separation applications because of the high selectivities obtained.

5. Conclusion

In order to investigate the possible enhancement of hydrogen and other gas separation properties, zeolite 4A nanoparticles with particle size of 50–120 nm were synthesised to use as the inorganic filler in flat-sheet mixed-matrix membrane fabrication. Flexible PVAc with a high affinity to zeolite 4A was used as the polymer matrix. Although MMMs with lower zeolite nanoparticle loading showed some agglomeration of nanoparticles without void formation, MMM with 40 wt% zeolite 4A nanoparticles were well dispersed throughout the PVAc phase. FTIR spectra of the membranes showed good interaction of the PVAc with the zeolite 4A nanoparticles. Thermal stability of the membranes was improved by increasing the zeolite content. In addition, the T_g increased by about 6 °C compared to the pure PVAc membrane, indicating the effective interaction of the zeolite nanoparticles and PVAc and rigidification of the polymer at the zeolite-polymer interface. Pure-gas permeability measurements with He, H_2, CO_2 and N_2 were performed to investigate the gas separation performance of the fabricated membranes. The effect of nano-sized zeolite 4A loading and temperature was also studied. The addition of zeolite nanoparticles to the PVAc matrix decreased the permeabilities of all the gases employed, with an increase in selectivities. The N_2 and CO_2 permeabilities decreased more than those of the smaller gas molecules He and H_2, showing the effectiveness of zeolite 4A nanoparticles as a molecular sieve. The permeabilities of all gases in all membranes increased by increasing the temperature from 30 °C to 50 °C. N_2, with the highest activation energy, was most affected by temperature increase, leading to a decrease in selectivities.

As nano-sized zeolite is not commercial available and the synthesis is expensive, a low zeolite content is more desirable. Unfortunately, the lowest zeolite composition (15 wt%) showed some agglomeration with lower permselectivity than the MMM

containing 40 wt% nanoparticles. To improve the dispersion in PVAc polymer during mixed matrix membrane fabrication with lower zeolite nanoparticle content, zeolite 4A nanoparticles were modified by silanation after synthesis. NMR spectroscopy, TGA and FTIR confirmed the silanation of the zeolite nanoparticles. Thermal stability of the membrane containing 15 wt% modified zeolite 4A nanoparticles was improved, compared to both the pure PVAc membrane and MMM with 15 wt% unmodified zeolite 4A nanoparticles. The T_g of the modified MMM was slightly lower than that of the unmodified MMM, demonstrating lower polymer-zeolite interface rigidification. Modification of the zeolite nanoparticles resulted in a decreased permeability and increased selectivity of the 15 wt% modified MMM, compared to the 15 wt% unmodified MMM. This could be attributed to the partial pore blockage by silane, which was supported by a reduction in BET surface area of the nanoparticles after modification. The permeabilities of the membrane with 15 wt% modified zeolite 4A nanoparticles were higher than the permeability of the MMMs containing 40 wt% unmodified zeolite 4A nanoparticles, with only slightly lower selectivities. Therefore, the modification of the zeolite by silanation has enabled the use of lower content of zeolite nanoparticles, due to less agglomeration, without decrease in permselectivity, and this resulting in more flexible membranes, due to the lower zeolite content.

This work has demonstrated the advantages of nano-sized zeolite over micron-sized zeolite as the filler for PVAc-based mixed matrix membranes. For low zeolite content, where agglomeration of the zeolite is observed, silanation is a suitable technique to improve filler-polymer interaction and reduce agglomeration. The silanated 15 wt% nano-sized zeolite mixed matrix membranes demonstrated the best gas permselectivities.

Acknowledgements

NE acknowledges receipt of Griffith University Postgraduate Research and Griffith University International Postgraduate Research scholarships.

Keywords: gas separation • membranes • silanation • nanosized • zeolites

Table 4. gas separation performance of the MMMs in literature containing nano-sized zeolite and various polymers, in addition to MMMs containing PVAc and zeolite 4A

					Permeability (Barrer)					selectivity				
Polymer	Zeolite	Particle size (μm)	Zeolite loading (wt%)	Operating conditions	He	H_2	CO_2	N_2	O_2	H_2/N_2	H_2/CO_2	CO_2/N_2	He/N_2	He/CO_2	O_2/N_2
PVAc [21a]	4A	0.5-1.5	50 (v%)	35 °C 220 psi mixed gas			11.5								
PVAc [30]	4A	1-5	25	303 K 8 bar pure gas		5.1	2.97	0.03	0.21	161.5	1.72	94			6.63
PVAc [6b]	4A	1-5	25	303 K, 8 bar (pure gas)		3.75	2.413	0.024	0.155	156	1.55	100.54			6.45
PVAc [15e]	4A	micron	15 (v%)						0.45						7.3-7.6
PI[a] [54]	Amino functionalised sodalite	0.105	35	25 °C (pure gas)		8				281					
Pebax-1657 [8a]	NaX	0.05-0.2	20	25 °C, 3 bar (pure gas)			32.3	0.33	2.6			98			7.8
PES[b] [23b]	4A	0.1	20	35 °C, 2 atm (He, H_2), 10 atm (other gases) (pure gas)	10.4	8.3	2.32	0.0907	0.583	91.51	3.58		114.66	4.48	6.43
PI [20c]	FAU/EMT (silanated)	0.5-0.8	25	35 °C, 150 psi (pure gas)			17.6								
PSF[c] [23a]	4A	0.03-0.16	25	Room temperature, (pure gas)				0.23	1.8						7.7
SPES[d] [22c]	4A	0.1	20	35 °C, 3.5 atm (H_2), 10 atm (other gases) (pure gas)	6.67	5.82	1.75	0.064	0.406	90.9	3.32	27.34	104.2	3.81	6.34
PDMS[e] [23c]	4A	0.08-0.25	40	35 °C, 5 bar (pure gas)			3208								
PES [15b]	SAPO-34	0.5-1	20 (w/w)	35 °C, 2 bar (pure gas)		7.06-12.57	1.53-5.12				2.45-4.64				
PI [55]	4A	0.105	20	35 °C, 4 atm (pure gas)			4.618	0.316				14.6			
	13X	0.125	30				11.215	0.225				49.8			
PES [19d]	BEA	0.1-0.3	20	35 °C, 2 atm (He), 10 atm (other gases)	11.7		4.13	0.141	0.825			29.3	83		5.85

				(pure gas)											
Matrimid® [56]	mesoporous ZSM-5	0.2	20	1100 Torr. (pure gas)		22.23	8.65	0.17	1.8	127.9	2.57				10.35
Ultem [57]	MFI (Grignard modified)	0.1, 0.3	20	35 °C, 2 atm (pure gas)			2.2								
PVAc (this work)	4A	0.05-0.12	40	303.15 K, 0.75 bar (pure gas)	7.02	4.85	0.76	0.032		151.56	6.38	23.75	219.37	9.23	
PVAc (this work)	Modified 4A by silane	0.05-0.12	15	303.15 K, 0.75 bar (pure gas)	8.15	5.55	0.907	0.0388		143.04	6.12	23.38	210.05	8.99	

[a]polyimide, [b]poly(ether sulfone), [c]polysulfone, [d]Sulfonated poly(ether sulfone), [e]Polydimethylsiloxane

References

[1] J. Chi, H. Yu, *Chin. J. Catal.* **2018**, *39*, 390–394.

[2] a) S. Kampouri, T. N. Nguyen, M. Spodaryk, R. G. Palgrave, A. Züttel, B. Smit, K. C. Stylianou, *Adv. Funct. Mater.* **2018**, *28*, 1806368–1806376; b) R. Mutschler, W. Luo, E. Moioli, A. Züttel, *Rev. Sci. Instrum.* **2018**, *89*, 114102–114110; c) A. S. Fedotov, D. O. Antonov, V. I. Uvarov, M. V. Tsodikov, *Int. J. Hydrogen Energy* **2018**, *43*, 7046–7054; d) H. Miyaoka, H. Miyaoka, T. Ichikawa, T. Ichikawa, Y. Kojima, *Int. J. Hydrogen Energy* **2018**, *43*, 14486–14492; e) N. Kirkaldy, G. Chisholm, J.-J. Chen, L. Cronin, *Chem Sci* **2018**, *9*, 1621–1626; f) F. Khalid, I. Dincer, M. A. Rosen, *Int. J. Hydrogen Energy* **2018**, *43*, 9112–9118.

[3] a) D. Bastani, N. Esmaeili, M. Asadollahi, *J. Ind. Eng. Chem. (Seoul, Repub. Korea)* **2013**, *19*, 375-393; b) Y. Zhang, J. Sunarso, S. Liu, R. Wang, *Int. J. Greenhouse Gas Control* **2013**, *12*, 84–107; c) M. Rezakazemi, A. E. Amooghin, M. M. Montazer-Rahmati, A. F. Ismail, T. Matsuura, *Prog. Polym. Sci.* **2014**, *39*, 817–861; d) C. E. Powell, G. G. Qiao, *J. Membr. Sci.* **2006**, *279*, 1–49.

[4] L. M. Robeson, *J. Membr. Sci.* **2008**, *320*, 390–400.

[5] M. J. Muñoz-Aguado, M. Gregorkiewitz, *J. Membr. Sci.* **1996**, *111*, 7–18

[6] a) J.-T. Chen, C.-C. Shih, Y.-J. Fu, S.-H. Huang, C.-C. Hu, K.-R. Lee, J.-Y. Lai, *Ind. Eng. Chem. Res.* **2014**, *53*, 2781−2789; b) J. Ahmad, M.-B. Hägg, *J. Membr. Sci.* **2013**, *427*, 73–84.

[7] a) D. R. Paul, D. R. Kemp, *J. Polym. Sci.* **1973**, *41*, 79–93; b) Q. Xue, X. Pan, X. Li, J. Zhang, Q. Guo, *Nanotechnology* **2017**, *28*, 065702–065711; c) A. Jamil, O. P. Ching, A. M. Shariff, *Appl. Clay Sci.* **2017**, *143*, 115–124; d) L. Ge, R. Lin, L. Wang, T. E. Rufford, B. Villacorta, S. Liu, L. X. Liu, Z. Zhu, *Sep. Purif. Technol.* **2017**, *173*, 63–71; e) G. Liu, Y. Labreche, V. Chernikova, O. Shekhah, C. Zhang, Y. Belmabkhout, M. Eddaoudi, W. J. Koros, *J. Membr. Sci.* **2018**, *565*, 186–193; f) N. Jusoh, Y. F. Yeong, K. K. Lau, A. M. Shariff, *J. Membr. Sci.* **2017**, *525*, 175–186; g) N. Jusoh, Y. F. Yeong, K. K. Lau, A. M. Shariff, *J. Cleaner Prod.* **2017**, *149*, 80–95.

[8] a) K. Zarshenas, A. Raisi, A. Aroujalian, *J. Membr. Sci.* **2016**, *510*, 270–283; b) A. Fernández-Barquín, C. Casado-Coterillo, M. Palomino, S. Valencia, A. Irabien, *Chem. Eng. Technol.* **2015**, *38*, 658–666.

[9] H. Sun, T. Wang, Y. Xu, W. Gao, P. Li, Q. J. Niu, *Sep. Purif. Technol.* **2017**, *177*, 327–336.

[10] Y. Liu, G. Liu, C. Zhang, W. Qiu, S. Yi, V. Chernikova, Z. Chen, Y. Belmabkhout, O. Shekhah, M. Eddaoudi, W. Koros, *Adv. Sci. (Weinheim, Ger.)* **2018**, 1800982–1800986.

[11] S. Quan, S. W. Li, Y. C. Xiao, L. Shao, *Int. J. Greenhouse Gas Control* **2017**, *56*, 22–29.

[12] C.-Y. Liang, P. Uchytil, R. Petrychkovych, Y.-C. Lai, K. Friess, M. Sipek, M. M. Reddy, S.-Y. Suen, *Sep. Purif. Technol.* **2012**, *92*, 57–63.

[13] B. Zornoza, C. Téllez, J. Coronas, O. Esekhile, W. J. Koros, *AIChE J.* **2015**, *61*, 4481–4490.

[14] a) J.-M. Duval, B. Folkers, M. H. V. Mulder, G. Desgrandchamps, C. A. Smolders, *J. Membr. Sci.* **1993**, *80*, 189–198; b) Ş. B. Tantekin-Ersolmaz, Ç. Atalay-Oral, M. Tatlıer, A. Erdem-Şenatalar, B. Schoeman, J. Sterte, *J. Membr. Sci.* **2000**, *175*, 285–288.

[15] a) X. Y. Chen, O. G. Nik, D. Rodrigue, S. Kaliaguine, *Polymer* **2012**, *53*, 3269–3280; b) E. Karatay, H. Kalıpçılar, L. Yılmaz, *J. Membr. Sci.* **2010**, *364*, 75–81; c) Y. Li, H.-M. Guan, T.-S. Chung, S. Kulprathipanja, *J. Membr. Sci.* **2006**, *275*, 17–28; d) Y. Li, T.-S. Chung, Z. Huang, S. Kulprathipanja, *J. Membr. Sci.* **2006**, *277*, 28–37; e) R. Mahajan, W. J. Koros, *Ind. Eng. Chem. Res.* **2000**, *39*, 2692–2696; f) G. Clarizia, C. Algieri, E. Drioli, *Polymer* **2004**, *45*, 5671–5681.

[16] a) H. Lee, **2005**; b) N. Esmaeili, H. Kazemian, D. Bastani, *Iran. J. Chem. Chem. Eng.* **2011**, *30*, 9–14.

[17] N. Esmaeili, H. Kazemian, D. Bastani, *Iran. J. Chem. Chem. Eng.* **2011**, *30*, 1–8.

[18] a) S. Alfaro, C. Rodríguez, M. A. Valenzuela, P. Bosch, *Mater. Lett.* **2007**, *61*, 4655–4658; b) O. Larlus, S. Mintova, T. Bein, *Microporous Mesoporous Mater.* **2006**, *96*, 405–412.

[19] a) A. L. Khan, A. Cano-Odena, B. Gutiérrez, C. Minguillón, I. F. J. Vankelecom, *J. Membr. Sci.* **2010**, *350*, 340–346; b) C. I. Chaidou, G. Pantoleontos, D. E. Koutsonikolas, S. P. Kaldis, G. P. Sakellaropoulos, *Sep. Sci. Technol.* **2012**, *47*, 950–962; c) J. K. Ward, W. J. Koros, *J. Membr. Sci.* **2011**, *377*, 75–81; d) Z. Huang, J.-F. Su, X.-Q. Su, Y.-H. Guo, L.-J. Teng, C. M. Yang, *J. Appl. Polym. Sci.* **2009**, *112*, 9–18; e) J.

Liu, J. Chen, X. Zhan, M. Fang, T. Wang, J. Li, *Sep. Purif. Technol.* **2015**, *150*, 257–267; f) X. Zhuang, X. Chen, Y. Sua, J. luo, W. Cao, Y. Wan, *J. Membr. Sci.* **2015**, *493*, 37–45; g) T. H. Nguyen, H. Gong, S. S. Lee, T.-H. Bae, *ChemPhysChem* **2016**, *17*, 3165–3169; h) G. Sodeifian, M. Raji, M. Asghari, M. Rezakazemi, A. Dashti, *Chin. J. Chem. Eng.* **2019**, *27*, 322–334.

[20] a) P. Wei, X. Qu, H. Dong, L. Zhang, H. Chen, C. Gao, *J. Appl. Polym. Sci.* **2013**, *128*, 3390–3397; b) R. Mahajan, R. Burns, M. Schaeffer, W. J. Koros, *J. Appl. Polym. Sci.* **2002**, *86*, 881–890; c) O. G. Nik, X. Y. Chen, S. Kaliaguine, *J. Membr. Sci.* **2011**, *379*, 468–478.

[21] a) R. T. Adams, J. S. Lee, T.-H. Bae, J. K. Ward, J. R. Johnson, C. W. Jones, S. Nair, W. J. Koros, *J. Membr. Sci.* **2011**, *367*, 197–203; b) T. T. Moore, W. J. Koros, *J. Mol. Struct.* **2005**, *739*, 87–98.

[22] a) O. M. Ekiner, S. S. Kulkarni, *Vol. US 6,663,805 B1* Air Liquide SA US, **2003**; b) L. Y. Jiang, T. S. Chung, S. Kulprathipanja, *J. Membr. Sci.* **2006**, *276*, 113–125; c) Y. Li, W. B. Krantz, T.-S. Chung, *AIChE J.* **2007**, *53*, 2470–2475.

[23] a) H. Wang, B. A. Holmberg, Y. Yan, *J. Mater. Chem.* **2002**, *12*, 3640–3643; b) Z. Huang, Y. Li, R. Wen, M. M. Teoh, S. Kulprathipanja, *J. Appl. Polym. Sci.* **2006**, *101*, 3800–3805; c) M. Rezakazemi, K. Shahidi, T. Mohammadi, *Int. J. Hydrogen Energy* **2012**, *37*, 14576–14589; d) B. Moermans, W. D. Beuckelaer, I. F. J. Vankelecom, R. Ravishankar, J. A. Martens, P. A. Jacobs, *Chem. Commun. (Cambridge, U. K.)* **2000**, 2467–2468.

[24] E. M. Mahdi, J.-C. Tan, *J. Membr. Sci.* **2016**, *498*, 276–290.

[25] a) Y. Zhang, I. H. Musselman, J. P. Ferraris, K. J. B. Jr., *J. Membr. Sci.* **2008**, *313*, 170–181; b) F. Dorosti, M. R. Omidkhah, M. Z. Pedram, F. Moghadam, *Chem. Eng. J. (Lausanne)* **2011**, *171*, 1469–1476.

[26] E. V. Perez, K. J. B. Jr., J. P. Ferraris, I. H. Musselman, *J. Membr. Sci.* **2009**, *328*, 165–173.

[27] a) A. E. Amooghin, M. Omidkhah, A. Kargari, *J. Membr. Sci.* **2015**, *490*, 364–379; b) S. Kango, S. Kalia, A. Celli, J. Njuguna, Y. Habibi, R. Kumar, *Prog. Polym. Sci.* **2013**, *38*, 1232–1261; c) H. H. Yong, H. C. Park, Y. S. Kang, J. Won, W. N. Kim, *J. Membr. Sci.* **2001**, *188*, 151–163.

[28] a) N. N. R. Ahmad, H. Mukhtar, D. F. Mohshim, R. Nasir, Z. Man, *Rev. Chem. Eng.* **2016**, *32*, 181–200; b) J.-Y. Kim, J. Kim, S.-T. Yang, W.-S. Ahn, *Fuel* **2013**, *108*, 515–520; c) M. U. M. Junaidi, C. P. Khoo, C. P. Leo, A. L. Ahmad, *Microporous Mesoporous Mater.* **2014**, *192*, 52–59.

[29] M. Jafari, A. Nouri, M. Kazemimoghadam, T. Mohammadi, *Powder Technol.* **2013**, *237*, 442–449.

[30] J. Ahmad, M.-B. Hägg, *Sep. Purif. Technol.* **2013**, *115*, 163–171.

[31] S. N. Azizi, A. R. Dehnavi, A. Joorabdoozha, *Mater. Res. Bull.* **2013**, *48*, 1753–1759.

[32] a) M. Salavati-Niasari, *Polyhedron* **2009**, *28*, 2321–2328; b) S. Khemakhem, R. B. Amar, *Colloids Surf., A* **2011**, *387*, 79–85.

[33] G. Clarizia, C. Algieri, A. Regina, E. Drioli, *Microporous Mesoporous Mater.* **2008**, *115*, 67–74.

[34] H. v. Bekkum, E. M. Flanigen, P. A. Jacobs, J. C. Jansen, *Introduction to zeolite science and practice*, 2nd Edition ed., **2001**.

[35] a) R. S. Murali, A. F. Ismail, M. A. Rahman, S. Sridhar, *Sep. Purif. Technol.* **2014**, *129*, 1–8; b) Y. Zhan, X. Li, Y. Zhang, L. Han, Y. Chen, *Ceram. Int.* **2013**, *39*, 5997–6003.

[36] a) A. F. Ismail, T. D. Kusworo, A. Mustafa, *J. Membr. Sci.* **2008**, *319*, 306–312; b) D. L. Pavia, G. M. Lampman, G. S. Kriz, J. R. Vyvyan, *Introduction to Spectroscopy*, 4th ed., Brooks/Cole, Belmont, CA, **2009**.

[37] O. G. Nik, B. Nohair, S. Kaliaguine, *Microporous Mesoporous Mater.* **2011**, *143*, 221–229.

[38] M. Füllbrandt, P. J. Purohit, A. Schönhals, *Macromolecules* **2013**, *46*, 4626−4632.

[39] K. B. R. Devi, R.Madivanane, *Engineering Science and Technology: An International Journal* **2012**, *2*, 2250–3498.

[40] A. F. Ismail, R. A. Rahim, W. A. W. A. Rahman, *Sep. Purif. Technol.* **2008**, *63*, 200–206.

[41] a) A.-L. Ciripoiu, A. Sarbu, C. Damian, A. Lungu, R. Gabor, H. Iovu, *Int. J. Polym. Anal. Charact.* **2012**, *17*, 568–577; b) R. Xing, W. S. W. Ho, *J. Taiwan Inst. Chem. Eng.* **2009**, *40*, 654–662; c) J. Ahmad, M.-B. Hägg, *Sep. Purif. Technol.* **2013**, *115*, 190–197; d) L. Lin, A. Wang, M. Dong, Y. Zhang, B. He, H. Li, *J. Hazard. Mater.* **2012**, *203–204*, 204–212.

[42] B. J. Holland, J. N. Hay, *Polymer* **2002**, *43*, 2207–2211.
[43] L. Clerc, L. Ferry, E. Leroy, J.-M. Lopez-Cuesta, *Polym. Degrad. Stab.* **2005**, *88*, 504–511.
[44] N. Grassie, I. F. McLean, I. C. McNeill, *Eur. Polym. J.* **1970**, *6*, 679–686.
[45] Y. Li, T.-S. Chung, C. Cao, S. Kulprathipanja, *J. Membr. Sci.* **2005**, *260*, 45–55.
[46] T.-S. Chung, S. S. Chan, R. Wang, Z. Lu, C. He, *J. Membr. Sci.* **2003**, *211*, 91–99.
[47] R. Mahajan, W. J. Koros, *Polym. Eng. Sci.* **2002**, *42*, 1432–1441.
[48] a) D. Sen, H. Kalipcilar, L. Yilmaz, *Desalination* **2006**, *200*, 222–224; b) X. Qiao, T.-S. Chung, R. Rajagopalan, *Chem. Eng. Sci.* **2006**, *61*, 6816–6825.
[49] S. Kim, E. Marand, *Chem. Mater.* **2006**, *18*, 1149–1155.
[50] P. Burmann, B. Zornoza, C. Téllez, J. Coronas, *Chem. Eng. Sci.* **2014**, *107*, 66–75.
[51] J. Xiao, J. Wei, *Chem. Eng. Sci.* **1992**, *47*, 1143–1159.
[52] M. Mulder, *Basic principles of membrane technology*, Kluwer Academic Publishers, Dordrecht, Netherland, **1996**.
[53] X. He, J. A. Lie, E. Sheridan, M.-B. Hägg, *Ind. Eng. Chem. Res.* **2011**, *50*, 2080–2087.
[54] D. Li, H. Y. Zhu, K. R. Ratinac, S. P. Ringer, H. Wang, *Microporous Mesoporous Mater.* **2009**, *126*, 14–19.
[55] H. Karkhanechi, H. Kazemian, H. Nazockdast, M. R. Mozdianfard, S. M. Bidoki, *Chem. Eng. Technol.* **2012**, *35*, 885–892.
[56] Y. Zhang, K. J. B. Jr, I. H. Musselman, J. P. Ferraris, *J. Membr. Sci.* **2008**, *325*, 28–39.
[57] T.-H. Bae, J. Liu, J. S. Lee, W. J. Koros, C. W. Jones, S. Nair, *J. Am. Chem. Soc.* **2009**, *131*, 14662–14663.

TOC

Nano-sized zeolite for mixed matrix membranes: Pure gas permeation measurements on PVAc mixed matrix membranes with nano-particular zeolite as the inorganic filler, demonstrate the advantages of nano-sizing the zeolite for gas separation applications. At low filler content levels, agglomeration of the nanoparticles was avoided by silanation of the zeolite before incorporation into the polymer.